ELSEVIER

Nuclear Instruments and Methods in Physics Research A 455 (2000) 346–360

NUCLEAR INSTRUMENTS & METHODS IN PHYSICS RESEARCH Section A

www.elsevier.nl/locate/nima

# Electromagnetic calorimeters for the BNL muon $(g-2)$ experiment

S.A. Sedykh[a], J.R. Blackburn[a], B.D. Bunker[a], P.T. Debevec[a], F.E. Gray[a], D.W. Hertzog[a,*], T.D. Jones[a], C.J.G. Onderwater[a], C.C. Polly[a], D.C. Urner[a], R.M. Carey[b], C. Coulsey[b], G. de Santi[b], M. Hare[b], J.P. Miller[b], J. Ouyang[b], O. Rind[b], A. Trofimov[b], P. Cushman[c], S. Giron[c], J. Kindem[c], C. Timmermans[c], D. Zimmerman[c], D. Winn[d], V. Druzhinin[e]

[a] *469 Loomis Laboratory of Physics, Department of Physics, University of Illinois at Urbana-Champaign, 1110 West Green Street, Urbana, IL 61801-3080, USA*

[b] *Department of Physics, Boston University, Boston, MA 02215, USA*

[c] *Department of Physics, University of Minnesota, Minneapolis, MN 55455, USA*

[d] *Department of Physics, Fairfield University, Fairfield, CT 06430, USA*

[e] *Budker Institute of Nuclear Physics, Novosibirsk, Russia*

Received 19 January 2000; received in revised form 23 May 2000; accepted 24 May 2000

**Abstract**

A set of 24 lead/scintillating fiber electromagnetic calorimeters has been constructed for the new muon $(g-2)$ experiment at the Brookhaven AGS. These calorimeters were designed to provide very good energy resolution for electrons up to 3 GeV while also yielding excellent timing information. Special requirements in the experiment related to the uniformity of response, the short-term gain and timing stability, and the neutron background led to several unusual design features. The calorimeters were tested and calibrated with electrons in the energy range 0.5–4.0 GeV and have been installed and used in the muon storage ring. The design criteria, construction, and performance of the system are described. 

*PACS:* 29.40.V; 13.35.B; 14.60.E

*Keywords:* Electromagnetic calorimeter; Lead scintillating fiber

## 1. Introduction

Experiment E821 at the Brookhaven AGS is designed to measure the anomalous magnetic moment of the muon to a precision of 0.35 ppm [1,2]. The E821 measurement follows the general scheme developed in the last CERN muon $(g-2)$ experiment [3]. The AGS provides, per cycle, up to $40\times10^{12}$ protons extracted in 6–12 bunches, each about 50 ns long. The interval between the bunches is about 30 ms. The proton beam is directed onto a production target, and a positive secondary beam is then transported to a 14.1 m diameter superferric

* Corresponding author. Tel.: 1-217-333-3988; fax: 1-217-333-1215.

*E-mail address:* hertzog@uiuc.edu (D.W. Hertzog).

0168-9002/00/$ - see front matter 
PII: S0168-9002(00)00576-3

storage ring with a highly uniform vertical magnetic field [4]. After injection, a bunch of polarized positive muons is trapped in the storage ring. The vertical focusing is provided by a set of electric quadrupoles [5]. The storage momentum of 3.094 GeV/$c$ is selected because at the "magic" $\gamma$ factor of 29.3 the muon spin precession is unaffected by the electric field. As the muons circulate the ring, the magnetic field precesses their spins in the horizontal plane such that the spin vector advances with respect to the momentum vector by $2\pi$ every 4.4 μs. The muons eventually decay, and the rate of the decays is observed by detecting the positrons using a set of calorimeters placed near the storage region. It is these calorimeters which are the subject of this report.

The calorimeters measure the energy and arrival time of the positrons. Because in the decay of muons the higher-energy positrons are preferentially emitted in the direction of the muon spin, the exponentially decreasing count rate of these positrons is modulated at the muon spin precession frequency. The decay electrons are detected during a time interval of approximately 700 μs following injection. This interval exceeds the dilated muon lifetime of 64.4 μs by more than a factor of 10.

In its essence the $(g-2)$ experiment is simply a count rate measurement, and the calorimeter signal is the only means to isolate the counts due to muon decay. Muons can be introduced into the storage ring in one of the two manners. Following the CERN $(g-2)$ experiment, the initial mode of operation of E821 used "pion injection". In this mode, the number of charged particles in each of the beam bunches brought into the ring is as high as $10^8$. About 63% of the beam particles are pions. As the pions begin to circle the ring, a small fraction of them, approximately 25 per million, decay leaving a muon with the correct momentum and trajectory to be stored. Many of the remaining pions, as well as the other particles in the beam (protons, muons, electrons), interact with the detectors and the magnet iron and create an enormous light burst in the detectors during a period of about 200 ns. In addition, a large number of spallation neutrons is created. Diffusion and thermalization of the neutrons lead to background signals in the detectors which extend for hundreds of microseconds, commensurate with the measuring period in the experiment. Reduction of this background was incorporated into the calorimeter design.

The second injection mode, referred to as "muon injection", represents one of the main improvements compared to the CERN experiment. Muon injection became available in 1998 during the second year of E821 operation. In this novel scheme, muons are injected directly into the ring and are placed on stored orbits by a fast magnetic kicker [6]. The efficiency of this injection scheme is significantly higher compared to pion injection, resulting in typically a 10-fold increase in the number of stored muons per injection. Further, the overall intensity of the beam which enters the $(g-2)$ ring at injection time is considerably lower. This translates into a 50-fold reduction in the neutron-induced background signals. Muon injection is currently used for data accumulation in E821.

To achieve the necessary precision on the muon anomalous magnetic moment measurement, systematic errors introduced by the experimental apparatus are to be kept below 0.1 ppm. The main subsystems which must be scrutinized in this regard are the muon storage ring magnet (field uniformity, absolute value, electric field), the decay electron detector and electronics systems. In this report, we describe the lead/scintillating fiber electromagnetic calorimeters which were built for this measurement. Several unique features were incorporated into the design to meet the peculiar environmental and systematic demands of the experiment.

After 12 of the 24 calorimeters were produced, they were tested at the Brookhaven AGS B2 test beam operated in fast-extraction mode. The detectors were subjected to 50 ns wide bursts of more than $10^7$ pions both into the calorimeters themselves and into mock-ups of the C-shaped magnet and yoke assembly surrounding them. These tests, performed at the AGS, demonstrated the existence of a long-lived background component due to neutrons thermalized inside the detectors themselves. This background was also seen in the CERN experiment and is initiated by those pions that strike massive obstructions in the ring during pion injection. In order to reduce this background, the remaining 12 detectors were doped with boron (see Section 4).

Following the development and refinement of a series of prototypes, the final calorimeters can be characterized as dense, fast, spatially uniform in response, and having moderate resolution. They are read out by photomultiplier tubes connected to base circuits designed to provide stable voltage to the dynodes, even under the condition of high count rate. Since the tubes are illuminated by an intense light flash during injection, each base has an internal switching circuit which temporarily disables the amplification during this period.

The absolute energy calibration of the calorimeters was performed in the BNL test beam and the relative calibration is preserved with the use of two systems. One is based on light-emitting diodes (LED), and the second uses a laser-illuminated fiber optic system. These calibration systems are also used to monitor short-term time and gain stability of the response of the calorimeters.

This paper begins with a description of how the key features of the muon $(g-2)$ experiment guided the calorimeter design. The remainder of the paper details the construction and performance of the calorimeters under both test beam and actual experimental conditions.

## 2. Design criteria

The energy spectrum of the positrons produced in the decay $\mu^+ \to e^+ \nu_e \bar{\nu}_\mu$ is described by the Michel spectrum in the center of mass. In the laboratory frame, the energy of the decay positrons is within the range 0–3.1 GeV. A positron with a momentum below the muon storage momentum of 3.094 GeV/$c$ curls to the inside of the storage ring where it exits through the gap in the C-shaped magnet and is recorded by one of the electromagnetic calorimeters distributed around the inside circumference. In order to avoid preshowering of the positrons as they exit the vacuum chamber, a novel scalloped design is used as shown in Fig. 1. Each positron signal is recorded by a 400 MHz waveform digitizer (WFD) which samples the photomultiplier output voltage versus time whenever the signal exceeds a preset hardware threshold. An offline analysis of a string of pulse samples is interpreted as the energy and time of arrival of a decay positron.

In a background-free environment, the spectrum recorded by the calorimeters is described by

$$N(t) = \int_{E_{\text{thr}}} n(E) e^{-t/\gamma\tau} [1 + A(E)\cos(\omega_a t + \phi(E))]\, dE \quad (1)$$

where the energy integral is over all positron energies above an energy threshold $E_{\text{thr}}$ in the laboratory frame system. The frequency $\omega_a$ represents the difference in the spin precession and cyclotron frequencies, and is directly proportional to the quantity of interest, namely $(g-2)$. This frequency is

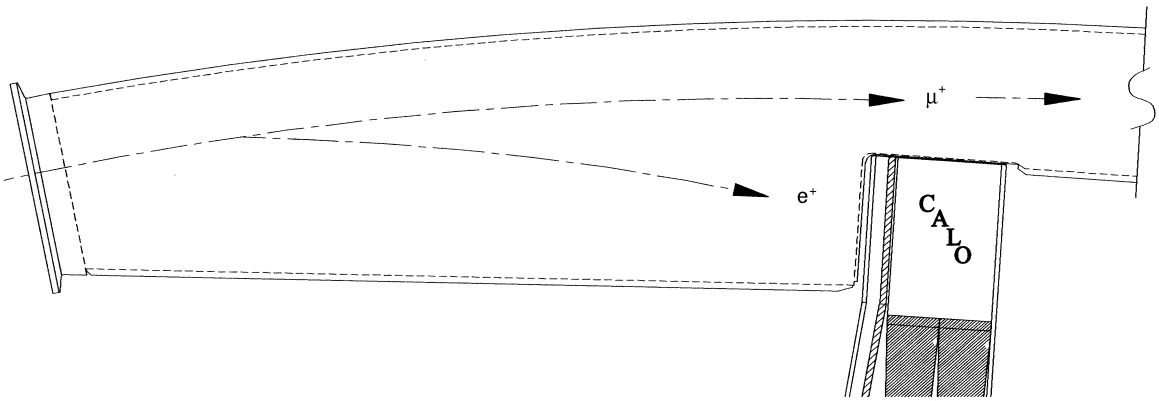


Fig. 1. Top view of the novel scalloped vacuum chamber and the location of the calorimeter. A decay positron curls to the inside of the ring and exits the vacuum chamber nearly orthogonally with respect to the vacuum chamber. This design reduces the effect of preshowering.

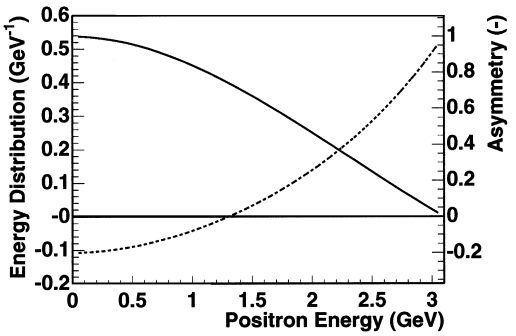


Fig. 2. The idealized energy distribution $n$ (solid; left scale) and the asymmetry $A$ (dashed; right scale) as a function of the decay positron energy.

extracted by fitting the accumulated time spectrum. The positron arrival time is therefore the primary measurement, imposing the twin constraints of fast signal risetime (for precision timing) and short pulse duration (to improve double hit rejection). This suggests the use of plastic scintillator-based detectors read out by photomultiplier tubes (PMTs).

The other parameters in Eq. (1) dictate the energy-related characteristics required of the calorimeter. The factor $n(E)$ represents the normalized acceptance fraction of the Michel spectrum as seen by a calorimeter, $A(E)$ is the energy-dependent asymmetry parameter in the weak decay, and $\phi(E)$ is the phase angle. The energy resolution and long-term gain stability requirements of the calorimeter system are modest because the energy resolution does not significantly affect the final statistical error in the $\omega_a$ measurement; if all positrons above $E_{\rm thr}$ are accepted while all those below are rejected, the calorimeter resolution simply affects the sharpness of the boundary. In Fig. 2, one can see that while $n(E)$ is a steeply falling function of energy, $A(E)$ is 1 for the highest energy positrons and drops to $-\frac{1}{3}$ at $E = 0$ crossing 0 at about 1.2 GeV.

The statistical error is inversely proportional to $\sqrt{\int_{E_{\rm thr}} n(E)A(E)^2}$, which is therefore clearly threshold dependent. The relative statistical error reaches its minimum when the energy threshold is set at about 1.8 GeV. In practice, a trigger-level hardware cut on the calorimeter signals is made at approximately 1.0 GeV. An offline software evaluation is used to make more precise energy cuts. When the threshold is set in the region $1.6 < E_{\rm thr} < 2.0$ GeV, the relative statistical error changes by only 4%. Therefore, a reasonable goal for the calorimeter energy resolution is 10% or better for $\sigma/E$ at the nominal threshold energy of 1.8 GeV.

Good energy resolution also determines the sharpness of the boundary above which only double-hit events can contribute. Such events have reconstructed energies above 3.1 GeV, originating from unresolved multiple hits. Understanding the shape of the high-energy part of the spectrum yields important information on the pile-up component of the overall fitting function (not indicated in Eq. (1). Finally, the statistical precision on $\omega_a$ can be improved using a maximum likelihood fit, weighting the data by positron energy, rather than applying a single energy threshold. The degree of improvement (up to 10%) also depends on the energy resolution.

Acceptance optimization for the high-energy positrons is achieved by instrumenting the 44 m long inside circumference of the storage ring with 24 compact detector stations distributed at uniform intervals. The height of the calorimeter is limited by the size of the opening in the gap of the C-shaped magnet. The depth of the calorimeter (defined in the azimuthal direction) is sufficient to contain 1–3 GeV electromagnetic showers. Since positrons below $E_{\rm thr}$ are not used in the analysis, yet contribute to the overall event rate in the calorimeter, it is desirable to reduce their acceptance. This can be done by keeping the radial size (and depth) of the calorimeter small enough that the low-energy positrons, which generally exit the ring at larger angles, curl between stations and are missed.

The gain and timing stability is also a concern, because the instantaneous event rate of a few MHz which occurs immediately after the injection, drops by almost five orders of magnitude during the 700 μs measuring period. This could result in a rate-dependent (and therefore time-dependent) response of the system. A gain shift $\Delta G$ in combination with a fixed threshold has the effect of changing the observed asymmetry $A$ and phase $\phi$ versus time; this in turn changes the extracted value of $\omega_a$. A time shift $\Delta T$ directly changes the fitted frequency. Gain and time stability concerns must be

addressed in three areas: (1) calorimeter materials and construction; (2) PMT/base intrinsic stability; and (3) WFD stability. The latter two will be discussed in separate reports. The overall gain and timing benchmarks are severe. The stability conditions which ensure less than a 0.1 ppm shift to $\omega_a$ are $\Delta G < 0.2\%$ and $\Delta T < 20$ ps over 200$\mu$s [1].

The uniformity of response versus horizontal impact position on the calorimeter front face has only a modest influence on the effective gain stability during the measuring interval. The average horizontal impact position moves radially outward approximately 0.5 mm during the measuring interval. This is caused by the slightly larger time-dilated lifetime of muons stored at larger radii compared to those stored at smaller radii. Horizontal uniformity better than 20% over 20 cm of the front face eliminates this concern. A higher degree of horizontal uniformity is necessary to maintain good energy resolution independent of impact position.

A detector which meets all of the above criteria is a dense sampling calorimeter made from polystyrene-based scintillating fibers embedded in a lead alloy (Pb/SciFi) [7]. Each station consists of a calorimeter module and a five-fold vertically segmented scintillator hodoscope, (see Fig. 3). On several stations, a higher granularity hodoscope with both vertical and horizontal segmentation was also used [8]. Each calorimeter is 22.5 cm wide $\times$ 14 cm high $\times$ 15 cm deep and is made of custom

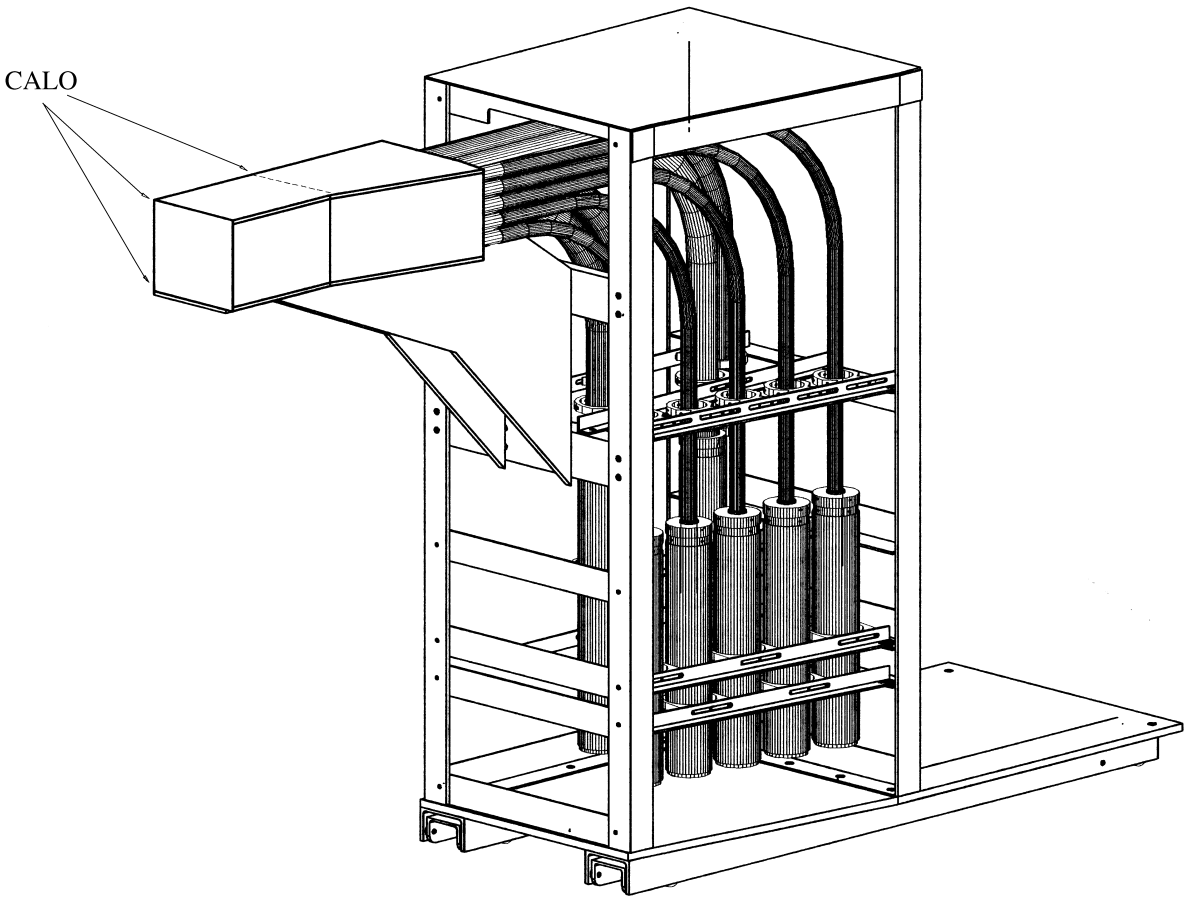


Fig. 3. A detector station including support structures, lightguides, and the iron housings which enclose the photomultiplier tubes and bases. The "snout" of the system plunges into the gap in the C magnet of the muon storage ring.

1 mm diameter Bicron BCF-99-49A fibers developed originally for our purpose from a fluor used in BC-404 fast timing scintillator. The fibers are oriented radially with respect to the storage ring such that the high-energy positrons enter the module nearly orthogonal to the fiber's length. To reduce the effect of the side-entering positrons while securing good electromagnetic shower containment, the plastic-to-volume ratio was adjusted to yield a radiation length $X_0$ of 1.14 cm.

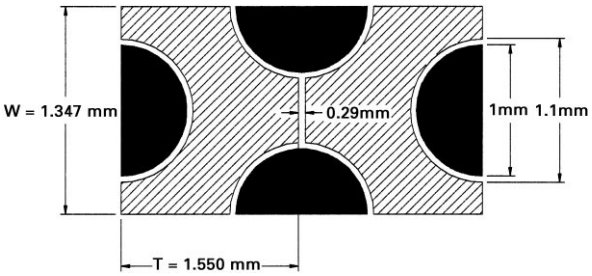


Fig. 4. Unit cell of fibers and Pb/Sb plates with final dimensions as measured from a completed sample.

## 3. Construction details

Following the Jetset electromagnetic calorimeter development [7], the Pb/SciFi material was assembled into a block from pre-grooved lead alloy plates ( $\approx 6\%$ antimony by weight) using a fiber weaving machine and an optical epoxy.[1] The uniformly spaced half-cylinder grooves in each plate have a diameter of 1.1 mm; the fiber diameter is 1.0 mm. In the assembly process, the liquid epoxy surrounds the fiber naturally and cures in place during a 24 h period while the block is held under moderate pressure. For the $(g-2)$ experiment, this design was modified to yield a shorter radiation length. This was accomplished by thickening the lead plates without changing the fiber pitch. The effect introduces a slight non-uniformity in the fiber placement as shown in Fig. 4. The dimensions are representative of a completed Pb/SciFi sample, including a thin glue layer placed between the flat portions of adjacent layers. Complementing this drawing is an actual fiber placement image of a completed block as seen in Fig. 5. This image was made by scanning an ultraviolet light pen[2] across the outer region of the module. The position of this pen was controlled to a precision of 0.13 mm. The current of the PMT versus pen position is plotted.

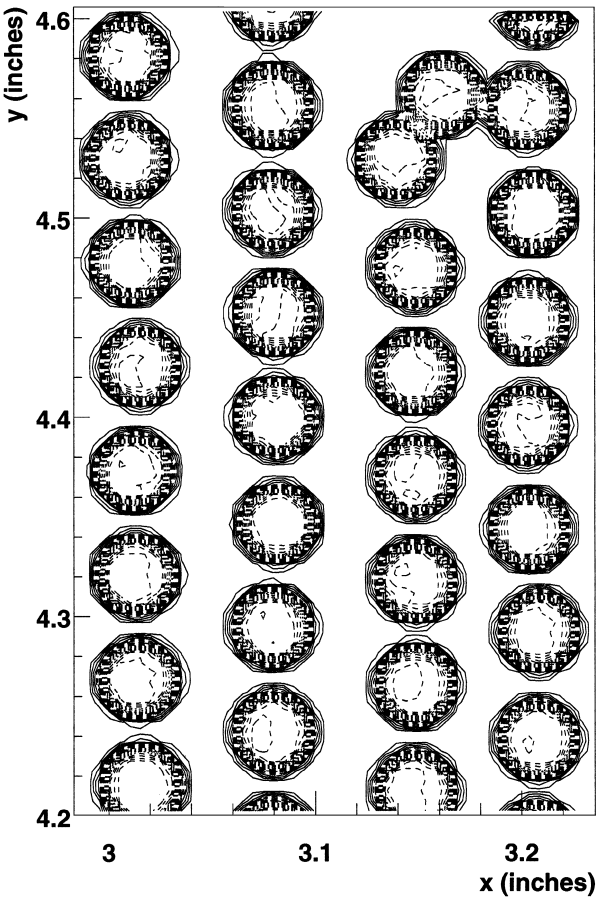


Fig. 5. Image of fiber grid for a small portion of one Pb/SciFi block created by scanning a DC UV light source across the fibers in 0.13 mm steps and recording the PMT current versus position of source.

[1] Stycast 1266 optical epoxy; Emerson Cummings Corporation.

[2] A Hg(Ar) spectral calibration lamp with an output at 253.7 nm was used with a long-wavelength conversion filter to generate a spectrum in the 320–400 nm range. The light was transported by a quartz fiber whose precise movement was controlled by a lightguide scanner.

The slight irregularities are typical of the construction process. At the top right in the figure, the image shows that one fiber has jumped from its groove. This was relatively rare. In the experimental setup the modules are oriented in such a way that, perpendicular to the incoming positron direction, an additional material appears on average as extra thin non-active vertical layers between planes of tightly packed fibers. The fractional composition for Pb : Sb : Fiber : Glue for one of the completed detectors is 0.466 : 0.049 : 0.369 : 0.096 (by volume). A calculation of the effective radiation length yields $X_0 = 1.144$ cm which implies that the 15 cm long detectors are 13 $X_0$ deep. In the 1–3 GeV energy region of interest for the $(g-2)$ experiment, this depth corresponds to a 93–96% shower containment fraction which is adequate for good energy resolution.

The 14 cm vertical height of the calorimeter exceeded the 9 cm maximum width of our plate rolling machine. To achieve a hermetic block, a technique was developed to place carefully trimmed lead foils side by side. For the first layer, two 7 cm wide plates were used. The next layer was composed of three plates. A 7 cm plate was placed in the center of the stack and two 3.5 cm wide plates were positioned to its side. This pattern was alternated to develop good constructional integrity. This procedure, along with the use of thicker plates, permitted use of existing tooling in order to make the Pb/SciFi modules appropriate for the muon $(g-2)$ experiment in a cost-effective and timely manner.

The anticipated high instantaneous rate in the calorimeter, coupled with the severe time and gain shift requirements eliminated all but 2 in. (or smaller) commercial photomultiplier tubes from consideration. A single 2 in. tube used to read out the whole calorimeter face cannot collect a sufficient fraction of the fiber light, nor can the uniformity of the light collection be obtained in a straight-forward manner. Subdivision of the readout face into four quadrants with one PMT per quadrant simplifies the problem because of the natural match between the fiber and photocathode areas. The light produced in the scintillating fibers from each quadrant is read out using a Hamamatsu R1828 photomultiplier tube. This 2 in. PMT features a low transit time jitter ( $< 240$ ps) and a fast risetime (1.3 ns) which are necessary characteristics for fast and stable timing.

The light from each quadrant is collected by an unwrapped and tapered 30 cm long UV-absorbing acrylic lightguide glued to the machined and polished surface of the Pb/SciFi block. This lightguide adiabatically reduces a 52.5 $cm^2$ rectangular area containing the termination points of the scintillating fibers to a 20.2 $cm^2$ circle. The circular cross section is preserved through an approximately 1 m long stock (UVT) acrylic rod which pipes the light to the PMT through a 90° bend. The bend in the rods was obtained by softening them in a 150° C oven and gently molding them around a form with a 25.4 cm radius of curvature (10 times the radius of the rod). The rods were annealed overnight at 90°C.

The polystyrene-based fiber core is surrounded by an acrylic cladding with indices of refraction ($n_{\text{core}} = 1.60$) and ($n_{\text{cladding}} = 1.49$), respectively. Consequently, the light cone into the lightguide has a maximum half-angle of

$$\theta_{\text{fibers}} \leq \arccos\frac{n_{\text{cladding}}}{n_{\text{core}}} = 21.4^\circ. \tag{2}$$

The acrylic-to-air interface determines the total internal reflection capture angle of the tapered light guides to be $\theta_{\text{guide}} < 47.8^\circ$. The entrance-to-exit area ratio for the light guides satisfies the condition for lossless transmission (in the adiabatic limit) as long as $A_{\text{in}}/A_{\text{out}} = (\sin\theta_{\text{guide}}/\sin\theta_{\text{fibers}})^2 < 4.1$ [7]. In our design, the reduction factor of 2.6 falls well within this criterion. The uniformity of the light collection, as measured across the input face of the guide was modeled and measured [9]. A profile of the measured light-collection efficiency is shown in Fig. 6. The vertical axis has been normalized to the light collection seen when the scintillating fiber used in the profile scan was centered directly on the front face of the PMT.

## 4. Neutron absorption

In addition to the signals from decay positrons, the calorimeter response contains pulses from

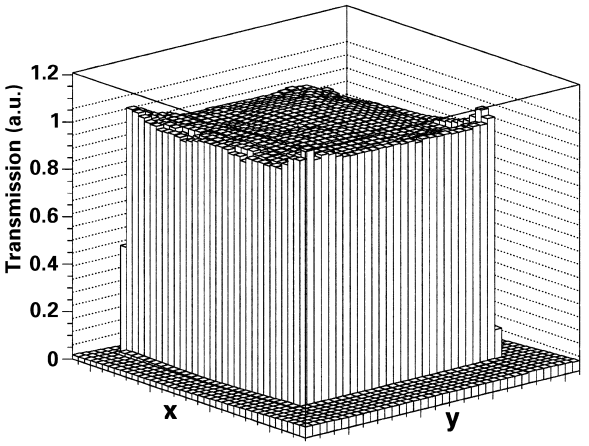


Fig. 6. Response of the PMT versus position of a single scintillating fiber scanned across the $7.0 \times 7.5\ cm^2$ entrance face of a tapered lightguide. The vertical axis represents relative transmission.

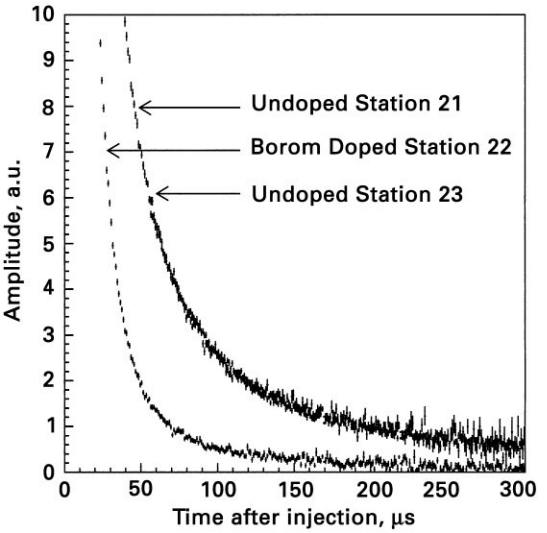


Fig. 7. The background level due to thermal neutron capture is plotted versus time following pion injection into the storage ring. Three adjacent detector stations are shown. Stations 21 and 23 were undoped. Station 22 included a 50% admixture of $B_4C$ powder into the epoxy. A significantly accelerated damping of the background is observed.

background due to thermalized neutrons. Detailed neutron diffusion Monte Carlo studies indicated that many of the neutrons thermalize in the detector, the lightguides, the magnet steel and the concrete floor. The time for this to occur follows a $1/t^n$ power law with $n \approx 1.5$–1.7.

Thermal neutrons produce two types of background. The first stems from direct neutron capture in the calorimeter Pb/SciFi block. Neutron-capture gamma rays produce an electron sea in the calorimeters which results in a slowly decreasing light output due to the pile-up of many small pulses. This background was expected from our flash tests, and action taken to reduce this effect consisted of introducing a fine powder into the epoxy surrounding the glue which was made from high-neutron-capture cross section nuclei such as $^{10}$B or $^{6}$Li. A prototype detector doped with $^{6}Li_2CO_3$ (lithium-6 carbonate) powder showed poor resolution and light output during test beam measurements. We do not understand the origin of this, but speculated that the cladding of the fibers might have been affected. A second prototype, prepared with a $^{10}B_4C$ (boron-10 carbide) powder worked well and we selected this doping for the production of the final 12 calorimeters. A small addition of boron into the detector materials accelerates the earlier capture of neutrons by the $n + {}^{10}B \rightarrow \alpha + {}^{7}Li + \gamma$ reaction. In a direct comparison, a boron-doped station was placed between two non-doped stations. The background in the boron-doped station was much more quickly damped, as can be seen by comparing the background light level versus time for the three stations shown in Fig. 7.

A second kind of background appeared unexpectedly in the 1997 pion-injection run as a series of very narrow, often high-amplitude, spikes in the PMT output signals. The count rate of these spikes followed a power-law behavior and extended for hundreds of microseconds. The amplitude spectrum reached the level corresponding to the height of the signals from multi-GeV electrons, while the width was uncharacteristically narrow, much like what is observed when one places a beta source directly on a photocathode surface. The possibility that the effect was entirely instrumental was ruled out by the observation that the relative strength of the background was smaller in the calorimeters with a higher photoelectron/GeV output. We concluded that such pulses must come directly from knock-out electrons in or near the photocathode.

Subsequent extended Monte Carlo studies showed that neutron captures in the concrete and steel of the magnet were responsible for providing a long-time source of such neutrons and that the solid angle to the photocathode was significantly high to account for the rate of this background. In order to reduce sensitivity to these narrow spikes, it was necessary to remove the yellow filters (see Section 5.4), thus increasing the true positron signal. It is important to note, however, that both neutron-induced backgrounds are reduced by a factor of 50 when the experiment is run in muon injection mode. In order to increase our true positron shower signal, compared to this photocathode background, modifications to increase the light coming from the detector were made as outlined in the discussion below on horizontal uniformity.

## 5. Performance

### 5.1. Test beam setup

The B2 test beam, operated in slow-extraction mode (essentially a continuous beam), was used to study prototypes and to make an absolute energy calibration of the detectors immediately prior to data taking in the $(g-2)$ ring.

The test beam measurements were carried out with a negatively charged beam consisting primarily of pions and electrons with user-selectable momenta from 0.5 to 5.0 GeV/$c$. Adjustable collimators permitted control of the beam rate and momentum spread. The priority in our adjustments of these collimators was adequate rate; the momentum varied with $\Delta P/P \approx 3\%$. A series of scintillator counters was used to define the trigger and to constrain the effective beam spot where the beam particles entered the calorimeter to an area of $1 \times 1$ cm$^2$. Electrons were distinguished from pions by a signal in a gas Cherenkov counter. Each of the PMT bases has two identical outputs. During data accumulation in the $(g-2)$ ring signals from one output were sent to the input of the WFD through high-quality RG-213 cables. The second output provided a signal into an analog-to-digital converter (ADC), and was used to monitor the response of the corresponding calorimeter quadrant to the calibration signals induced by the LED and laser systems. Similarly, in the test beam measurements, a signal from one photomultiplier output was sampled at a rate of 400 MHz by one of the waveform digitizers used in the actual experiment. This information was recorded to study the pulse shape as a function of energy and impact position. The signal from the other PMT output was sent to a LeCroy 2249A ADC. The trigger pulse generated by the coincidence of signals from the beam counters was used to open a 100 ns ADC gate.

The electron-to-pion ratio varies as a function of momentum with a typical value of 5% in the working range from 2.0 to 3.0 GeV used for most of the tests. The physical setup included a remotely adjustable detector platform which could translate the entire detector station transverse to the beam direction horizontally and vertically. The platform could also be rotated in order to position the detector in either "head-on" or "side-on" mode. In head-on mode, the beam entered nearly parallel to the fiber direction. A few-degree tilt prevented electrons from traversing long distances in the fibers prior to showering. Side-on mode represented the detector position relevant for the $(g-2)$ experiment, with the fibers aligned transverse to the beam direction.

In order to establish the proper photomultiplier gain, the detectors were first placed in the head-on position with the $1 \times 1$ cm$^2$ beam spot positioned, in turn, at the center of each quadrant. This arrangement ensured nearly full shower containment solely within one quadrant. By adjusting the high voltage of the PMTs, the response of each of the four quadrants to 2 GeV electrons was equalized with a precision of about 1%. The gain was set such that signals from 2 GeV electrons, summed at the input of the WFD, would correspond to 50% of the full WFD range. This gain was maintained while moving the calorimeters to the $(g-2)$ ring.

All relevant performance measurements were made in side-on mode immediately following establishment of the individual PMT high-voltage settings. In this position, individual showers were sampled by at least two and up to four of the PMTs depending on impact position. For each of the 24 pre-calibrated detectors, separate "top half" and "bottom half" studies were made with the beam entering 3.5 cm above or below the midplane at the

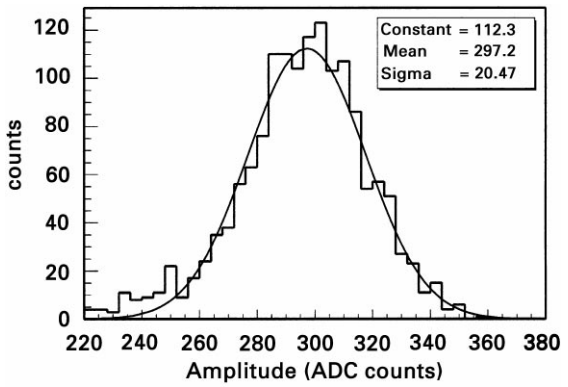


Fig. 8. Measured response of one of the calorimeters to 2 GeV electrons in the side-on mode.

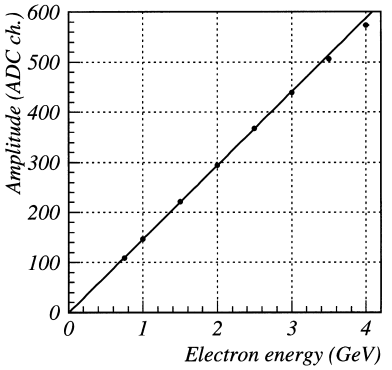


Fig. 9. The measured calorimeter response as a function of the electron energy in side-on mode.

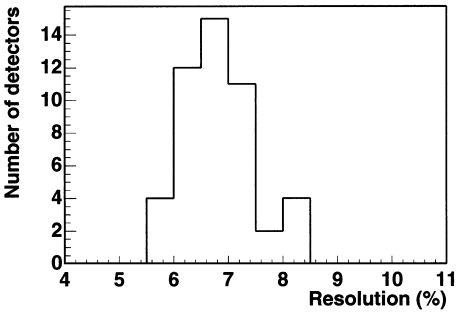


Fig. 10. Measured energy resolution distribution for 2 GeV electrons in side-on mode. Separate entries exist for the top and bottom halves of each of the 24 calorimeters.

radial midpoint along the fibers. A plot of the mean response of these 48 measurements had a RMS variation of 3.8%. The reasons for the additional width compared to the head-on adjustment are twofold. In the original calibration position, the $1 \times 1$ cm$^2$ beam spot sampled a specific set of fibers at near parallel incidence. Variations at the 1–2% level occur with slight changes in beam positioning or incident angle. Turned to the side, the calibration check is made with the beam striking midway along the fiber length. Different fiber groups are sampled, and differences in the attenuation lengths of quadrants accounted for an additional few percent variance.

The energy deposition spectrum for one of the detectors in the side-on position is shown in Fig. 8. The spectrum has a low-energy tail which can be explained mainly by shower leakage, but also includes contributions due to energy loss in trigger counters placed upstream of the calorimeter. The spectrum was fitted by a Gaussian curve. Fig. 9 depicts the calorimeter energy response linearity. The calorimeter has a linearity of better then 1% up to 3 GeV. The deviations from the linear form are 1.6% at 3.5 GeV and 2.5% at 4 GeV. They are accounted for by shower leakage through the back of the calorimeter.

### 5.2. Energy resolution

The distribution of the energy resolutions measured in the side-on mode for 2 GeV electrons entering the centers of the top and bottom halves of the calorimeters is shown in Fig. 10. At this energy, close to the nominal single-threshold of 1.8 GeV, the average resolution is $\sigma/E = 6.8\%$, including longitudinal losses. The number of photoelectrons (pe) per GeV was also determined for each quadrant. This estimation was made by measuring the relative width of the pulse-height distribution of LED signals, of which the amplitude corresponded to a 1 GeV electron pulse. The distribution of pe/GeV has an average of 550 and a RMS of 230. The spread in light collection efficiency was investigated during the series of tests and found to be mainly due to light losses in the tapered lightguides. For several of the calorimeters these lightguides were replaced which resulted in considerable improvement in light collection. As can be seen from

Fig. 10, in the final system every detector has a resolution better than 8.5% for 2 GeV electrons. This performance meets our design goal.

The dependence of the energy resolution versus energy was studied in detail for one of the calorimeter stations using both data and simulations. Three contributions are needed to describe the behavior. They include the sampling fluctuation term, a constant term and a longitudinal leakage correction factor. The constant term includes an uncertainty in the beam momentum. The sampling term includes the statistical fluctuations in the number of fibers crossed during shower development and the photostatistics term. The finite depth of the detector makes it necessary to introduce a longitudinal leakage correction factor as suggested in Fabjan's review of calorimeters [10]. This modifies the full-containment sampling term according to

$$\frac{\sigma(E)}{E} \simeq \left[\frac{\sigma(E)}{E}\right]_{f=0} \times [1 + 2f\sqrt{E}] \tag{3}$$

where $f$ represents the fractional loss due to the finite containment and $E$, the electron energy, is measured in GeV.

In order to evaluate the energy-dependent fractional loss, the calculated energy deposition profile [10] was integrated up to 13 radiation lengths for incoming electrons in the 1–5 GeV range. This provided an estimate of the fractional containment versus energy. A simple parameterization of the fractional loss function is $f(E) = 0.0147 + 0.0241E - 0.00197E^2$. In order to check the validity of this parameterization, the"back-to-front" ratio, i.e. the ratio of the amount of energy deposited in the back part of the calorimeter with respect that deposited in the front part, was also computed and compared to the data; in the test beam, signals from all four quadrants of the calorimeter are recorded by independent ADCs. This ratio of energy deposition in the front half of the calorimeter to the one in the back half is quite sensitive to depth in radiation lengths for each quadrant. The results are shown in Fig. 11 where it is evident that the calculation describes the data well.

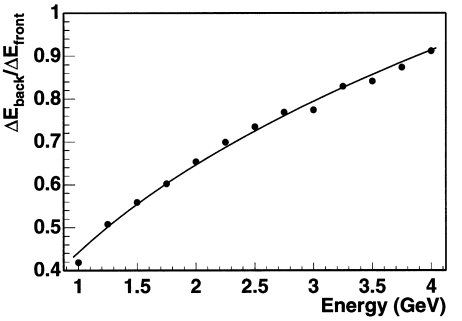


Fig. 11. Back-to-front ratio of energy deposition versus incident electron energy (data). The curve represents the result of a calculation which integrates the expected energy deposition assuming that front and back quadrants have equal depths in radiation lengths of 6.55 $X_0$.

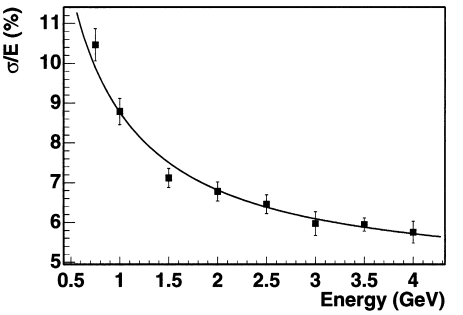


Fig. 12. The measured energy resolution, $\sigma_E/E$ in %, as a function of electron energy for one of the calorimeters in side-on mode. The fit is described in the text and includes sampling, constant and longitudinal leakage terms.

Given these preliminary steps, we can now fit the data which is shown in Fig. 12. The final result is well described by the expression

$$\sigma(E)/E = \sqrt{(1.7 \pm 0.5\%)^2 + \left[\frac{(8.0 \pm 0.3\%)}{\sqrt{E}}\right]^2} \times [1 + 2f(E)\sqrt{E}]. \tag{4}$$

In this parameterization, the factor containing $8.0 \pm 0.3\%$ is representative of the sampling and photoelectron statistics contributions assuming full containment. Folding out the contribution of photoelectron statistics, which for this detector is equal to 4.2%, implies an intrinsic sampling term of $6.8 \pm 0.3\%$ for our choice of fiber diameter and

placement, and under the assumption of full containment. The result of this estimate can be compared to a similar value for the Jetset Pb/SciFi calorimeters [7] developed by some of us previously which had an intrinsic resolution factor of 6.3%. However, the Jetset fiber density exceeds that for $(g-2)$ by the factor 62/47 and the intrinsic resolution factor scales approximately with the square root of number of fiber crossings. Thus, for $(g-2)$ the scaled sampling term factor, based on the Jetset experience, should rise to 7.2% which is consistent with the extracted result.

### 5.3. Vertical uniformity

The vertical uniformity profile is a measure of the overall detector construction integrity and of the losses which occur near the top and bottom edges and at the midplane, where the upper and lower quadrant lightguides meet. The flat faces of the upper and lower quadrant lightguides are pressed together with no material in between. This technique proved to be the best for overall light collection across the boundary and featured very high isolation between the guides. This interface might still be expected to induce a dip in the summed response when a shower is incident at the midplane. The effect is small having been reduced by the natural spreading of the shower and the size of the incident beam of about 1 cm $\times$ 1 cm. A vertical scan for one of the detectors is shown in Fig. 13. Only a tiny ( $\approx 1\%$) dip is observed at the center position. This dip was observed to be larger in a few of the calorimeters but was within 5% for all the stations. The roll-off at the top and bottom is due to leakage caused by the vertical extension of the shower. The non-uniform response does not change as a function of time after injection, even at the edges. Thus, as long as the geometrical distribution of the incident electrons does not radically shift from early-to-late times (as a result, for example, of a shift in the geometric distribution of the stored muons), no influence on $\omega_a$ is expected. Nevertheless, a high-degree of uniformity, as seen in most of these detectors, reduces any possible second-order effects. Fig. 14 shows the energy resolution for incident 2 GeV electrons versus vertical position.

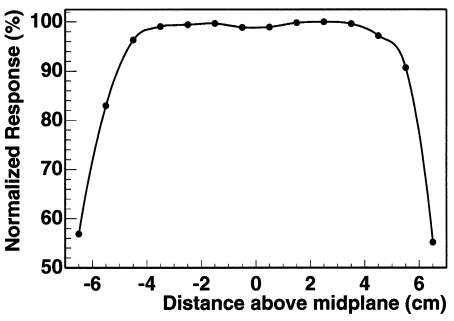


Fig. 13 . Measured normalized response for 2 GeV electrons incident on the calorimeter center versus vertical position.

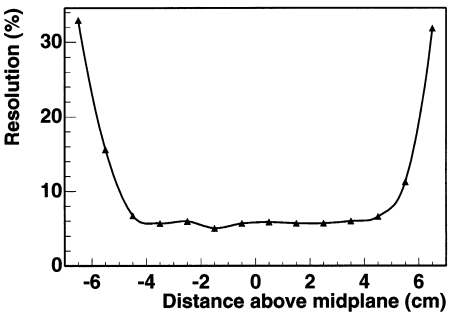


Fig. 14. Measured resolution versus vertical impact position for 2 GeV electrons incident on the calorimeter center in side-on mode.

A vertical uniformity parameter defined to quantify the consistency between the top and bottom half responses for each calorimeter is

$$\delta_{\mathrm{top-bottom}} = 2 \cdot \frac{A_{\mathrm{top}} - A_{\mathrm{bottom}}}{A_{\mathrm{top}} + A_{\mathrm{bottom}}} 100\% \qquad (5)$$

where $A$ represents the mean of the energy histogram produced when the beam entered the center of the top or bottom half as indicated by the subscript. The distribution of $\delta_{\mathrm{top-bottom}}$ for the 24 stations had a mean of $\delta_{\mathrm{top-bottom}} = -0.75\%$ and a RMS width of 2.6%, consistent with the 3.8% RMS spread observed when the detectors were turned from head-on to side-on mode as discussed above. Two stations had a top–bottom difference greater than 5%.

### 5.4. Horizontal uniformity

In the original design of the detectors, the calorimeter light collection system included a Kodak Wratten #2E "yellow" filter placed between the termination of the lightpipe and the PMT photocathode. This filter increased the effective attenuation length of the scintillating fiber by removing the high-frequency component of the light. Since it is just that component which suffers the strongest self-absorption, the yellow filters serve to make the calorimeter response more uniform as a function of distance from the light guide. Overall, the filter removed about 55% of the calorimeter light. The severity of the narrow spike background (see Section 4) in the pion-injection run was strongly correlated to detectors having the lowest photoelectron yield per GeV. Removing the filters in situ on some of the detectors during the run had the desired effect of doubling the light output from the real positrons while not changing the signal size of the background, indicating that the source of the spikes was at the surface of the tube itself.

To regain the horizontal uniformity advantage provided by the yellow filters, we investigated the idea of placing aluminized mirrors on the outward radial face of the detectors. A procedure was developed to apply a smooth layer of 3M-850 aluminized polyester tape to the outer surface of the block, having been prepared carefully through sanding and polishing stages to a final grit of 0.01 μm. With this introduction, an additional 30–50% increase in the photoelectron yield per GeV became available and the effective attenuation length of the detectors increased significantly compared to the no-reflection no-filter case. Therefore, in the final configuration the yellow filters were removed and the calorimeters were equipped with mirrors. The final response profile versus distance from the lightguides for one of the detectors is shown in Fig. 15. A horizontal uniformity parameter is defined by

$$\delta_{\text{horiz}} = \frac{A(4\text{ cm}) - A(20\text{ cm})}{A(12\text{ cm})}\ 100\% \qquad (6)$$

where $A(x)$ represents the amplitude of the mean at the position $x$ cm from the lightguide. A distribution of the $\delta_{\text{horiz}}$ values for the 48 top and bottom calorimeter halves has a mean of 4.9% with a RMS width of 1.8%.

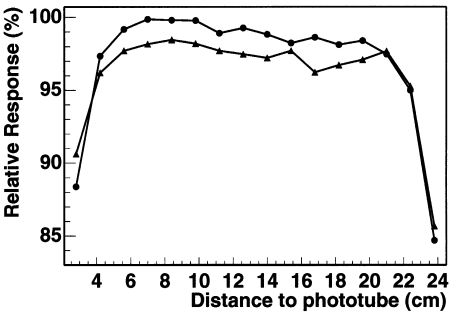


Fig. 15. Measured normalized response for 2 GeV electrons versus the distance from the light guide. The two sets of data correspond to the top and bottom half of the detector.

### 5.5. In-ring performance

Prior to the 1998 muon injection run, the 24 detector stations were recalibrated using the test beam and were then transported to the $(g-2)$ ring. A final magnetic field on/off adjustment of up to 12% was made for some of the PMT gains. The laser and LED systems were used to monitor the gain before and after such changes. Since waveform digitization was applied to the sum of pulses from the calorimeter quadrants, the timing of the four inputs into the WFD were adjusted carefully using the laser system and subsequently checked using decay positrons. As mentioned above, a signal amplitude from a 2 GeV positron shower in a calorimeter corresponds to the middle of the WFD full-scale range of 1 V. The average pulse shape, as recorded in the WFD for a sample of $\approx 2.0$ GeV electrons is shown in Fig. 16 where the nearly constant baseline is due to an artificial pedestal controlled by an adjustable input on the WFD. Due to the small width of the signal and the 2.5 ns sampling of the dual-phase 200 MHz WFD, the typical FWHM of the digitized signal is only 3 samples. The relatively course sampling introduces a reduction in the effective resolution of the signals. Analysis of the pulse shape data obtained with a WFD during the test beam calibration revealed that energy resolution remains at about the 8% level for 2 GeV signals when the integral of the

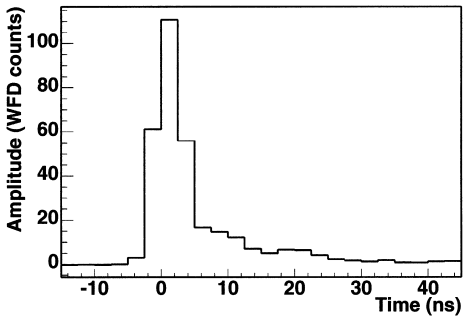


Fig. 16. Average measured pulse shape for 2 GeV electrons as digitized by the waveform digitizer in the test beam from the four input PMT signals.

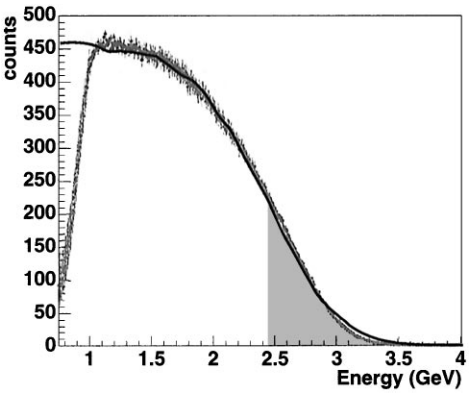


Fig. 17. Detector-averaged energy spectrum from decay electrons in the muon storage ring (data). A hardware threshold of approximately 1.0 GeV is observed on the low side. The histogram is calibrated in GeV by using the knowledge of the maximum electron energy convoluted with the detector energy resolution which comes from the Monte Carlo fit which is overlaid on the data. The gray shaded region represents the upper 10% of the spectrum which is used to establish a relative gain figure of merit for the detectors.

sampled pulse is extracted. Fluctuations in peak amplitudes of the pulses are much larger and reach 15% for 2 GeV electron signals.

The energy distribution of decay positrons striking each calorimeter is approximately the same for each station. Furthermore, the highest-energy electron entering any station is fixed at 3.1 GeV. Therefore, an absolute energy scale ("in-ring") can be made using the end-point information folded in with the detector resolution. The detector-averaged energy spectrum is shown in Fig. 17 scaled in units

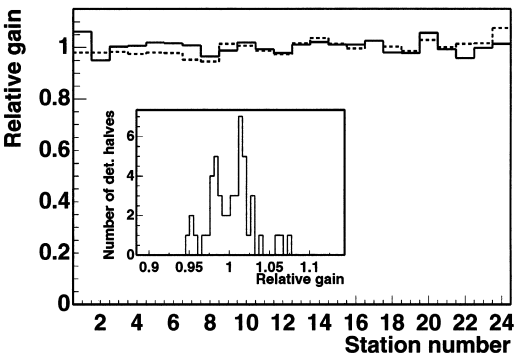


Fig. 18. Top and bottom half gains for the calorimeter stations following final adjustments in the $(g-2)$ ring.

of GeV. A GEANT Monte Carlo simulation is overlaid on the figure. The simulation is complete. It includes a realistic muon distribution in the ring, spin rotation and decay, all of the ring hardware, and full shower evolution in the Pb/SciFi detectors. In addition to the pulse samples for an individual electron shower, the WFD records which of the four input signals exceeds an independent tag-bit threshold. This tagging scheme allows one to select pulses which correspond to showers localized only in the top or only in the bottom half of the calorimeter. A figure of merit representing the relative gains of the detectors is made by starting at the highest energy recorded for each detector half and counting down for a fixed fraction of events as shown by the gray shaded region in Fig. 17. The gains of the individual station halves can then be compared using this figure of merit. When these distributions were first accumulated after the test beam, most of the stations were found to be in good agreement with each other and the top and bottom halves were properly balanced. These stations required no further gain adjustments. However, several stations demonstrated significant departures from the typical distribution, with quadrant gain imbalance as indicated by the LED ratio measurements. For these stations additional PMT gain corrections in the range 7–15% were made in addition to those required by the adjustments to compensate for the magnetic field effect. The final figure-of-merit results are plotted in Fig. 18. The inset plot shows the distribution of the 48 individual values and has a RMS of 2.7%.

For the data sample of decay positrons with energy above 1.8 GeV the observed asymmetry values $A(E_t)$ were measured to be approximately 0.37 for most of the stations in the ring. This can be compared to the theoretical value $A(1.8\ \text{GeV}) = 0.41$ for an ideal detector and to the average asymmetry of 0.28 for the same energy cut in the last muon $(g-2)$ experiment at CERN. Compared to the CERN experiment the main improvement is the inclusion of the special scallop-like vacuum chamber (see Fig. 1) which minimized the decay positron pre-showering. In addition, the asymmetry is improved by the higher energy resolution detectors used here. The lowest asymmetry value found in our present system was 0.33 and occurs at the two stations placed immediately downstream of the electrostatic kicker. These stations are subjected to additional positron pre-showering in the kicker plates. Since the statistical uncertainty in the extraction of $(g-2)$ is linearly proportional to $A$, the average improvement compared to CERN is significant.

## 6. Summary

An electromagnetic calorimeter system meeting the unique requirements posed by the muon $(g-2)$ experiment at Brookhaven has been designed, built and commissioned. A Pb/SciFi sampling calorimeter was selected for its particularly attractive characteristics: fast response, high density and good energy resolution. The 24 detector stations which comprised the complete system were each read out by four fast photomultiplier tubes and instrumented with custom gated bases. The summed signal was used as the final measurement in the experiment which placed considerable additional demands on the matching of the individual gains of the PMTs. Neutron-induced backgrounds, discovered in the mid-production phase, suggested several modifications including the doping of the detector materials with a high neutron capture cross section compound and the final mirroring of the outer radial face in order to increase the photoelectron yield per GeV. The final performance of the detectors is excellent and well within the benchmarks set in order to keep detector-induced systematic errors small.

## Acknowledgements

We thank the rest of our E821 collaborators for their many suggestions and encouragement. The AGS staff provided excellent support for numerous years of development and calibration in the B2 Test Beam. Early versions of the detector and assembly were built by Milco Moushmof and James Gabbard. This work was supported by the United States National Science Foundation and the Department of Energy.

## References

[1] BNL AGS E821 Collaboration Design Report, March 1995.
[2] R.M. Carey et al., Phys. Rev. Lett. 82 (1999) 1632.
[3] J. Bailey et al., Nucl. Phys. B150 (1979) 1.
[4] G.H. Danby et al., The Brookhaven muon storage ring magnet, Nucl. Instr. and Meth. (2000), in press.
[5] Y. Semertzidis et al., The Brookhaven muon storage ring high voltage quadrupoles, Nucl. Instr. and Meth., to be submitted.
[6] E. Efstathiadis et al., The $(g-2)$ Muon Kicker: specifications and performance of the final prototype, $(g-2)$. Internal Note 304, February 1998.
[7] D.W. Hertzog et al., Nucl. Instr. and Meth. A 294 (1990) 446.
[8] P. Cushman et al., Nucl. Instr. and Meth. A 378 (1996) 116.
[9] D. Simon et al., Nucl. Instr. and Meth. A 335 (1993) 86.
[10] C. Fabjan, Calorimetry in high-energy physics, in: T. Ferbel (Ed.), Experimental Techniques in High-Energy Nuclear and Particle Physics, 2nd Edition, World Scientific Publishing Co., Singapore, 1991, p. 257.